Evaluation of Microphysical Retrievals from Polarimetric Radar with Wind Profiler Data

PETER T. MAY AND THOMAS D. KEENAN

Bureau of Meteorology Research Centre, Melbourne, Victoria, Australia

(Manuscript received 27 May 2004, in final form 30 October 2004)

ABSTRACT

Polarimetric radar data have been used to produce microphysical classifications. This kind of analysis is run in a real-time mode from several research radars, including the C-band polarimetric (C-Pol) radar in Darwin, Australia. However, these classifications have had very little systematic evaluation with independent data. Using surface data is often difficult because of sampling issues, particularly for hail. The approach taken here is to use a combination of 50- and 920-MHz wind profiler estimates of rain and hail to provide validation data for the radar pixels over the profiler. The profilers also observe signals associated with lightning, and some comparisons are made between lightning occurrence and the radar measurements of graupel. The retrievals of hail–rain mixtures are remarkably robust; there are some issues regarding other microphysical classes, however, including difficulties in detecting melting snow layers in stratiform rain. These difficulties are largely due to the resampling of the radar volume data onto a grid and to poor separation of the snow classes.

1. Introduction

A number of groups are using polarimetric radar measurements to automatically estimate the microphysical type of the hydrometeors within a radar volume (e.g., Straka 1996; Straka et al. 2000; Vivekanandan et al. 1999; Keenan 2003). These applications hold much promise for both research and operational applications (e.g., Schuur et al. 2003). The algorithms that underpin these systems exploit the fact that different hydrometeor species occupy different parts of the polarimetric-variable phase space. However, these phase-space hypervolumes have significant overlapping areas. Therefore, fuzzy-logic approaches have been used to determine the best estimate of the hydrometeor species.

These algorithms are now being applied routinely at several centers, for example, at Colorado State University [University of Chicago–Illinois State Water Survey (CHILL) radar], the National Center for Atmospheric Research [S-band polarimetric (S-Pol) radar], the National Severe Storms Laboratory [Next-Generation Weather Radar (NEXRAD) upgrade project radars], and the Bureau of Meteorology Research Centre [BMRC; C-band polarimetric (C-Pol) radar]. These radars are all 10-cm-wavelength systems except the latter (C-Pol; Keenan et al. 1998), which has a radar wavelength of 5.5 cm. These data are being supplied in real time for field programs and, in the case of C-POL, to the wider community through the U.S. Department of Energy Atmospheric Radiation Measurement (ARM) Program (information is available online at http://www.arm.gov) as an external dataset associated with the Darwin, Australia, site. As these data become available, a significant question concerns their reliability. Testing the separation between snow and rain is relatively straightforward in the United States, and good success has been found (e.g., Schuur et al. 2003). However, hail and graupel are much harder to verify. Ground surveys of large hail are notoriously difficult and most efforts at verifying the polarimetric retrievals have effectively concluded that "the retrievals look reasonable." There are occasionally fortuitous observations that lend support to the retrievals. Figure 1 shows an RHI cross section through a very deep, intense thunderstorm over the Tiwi Islands, north of Darwin. The top panel shows the reflectivity. Note that there is a distinct flare echo extending behind the storm radially from an altitude of 4–5 km. Such flare echoes arise from multiple scattering of the radio waves and are an indi-

Corresponding author address: Dr. P. T. May, BMRC, GPO Box 1289K, Melbourne, 3001, Victoria, Australia.
E-mail: p.may@bom.gov.au

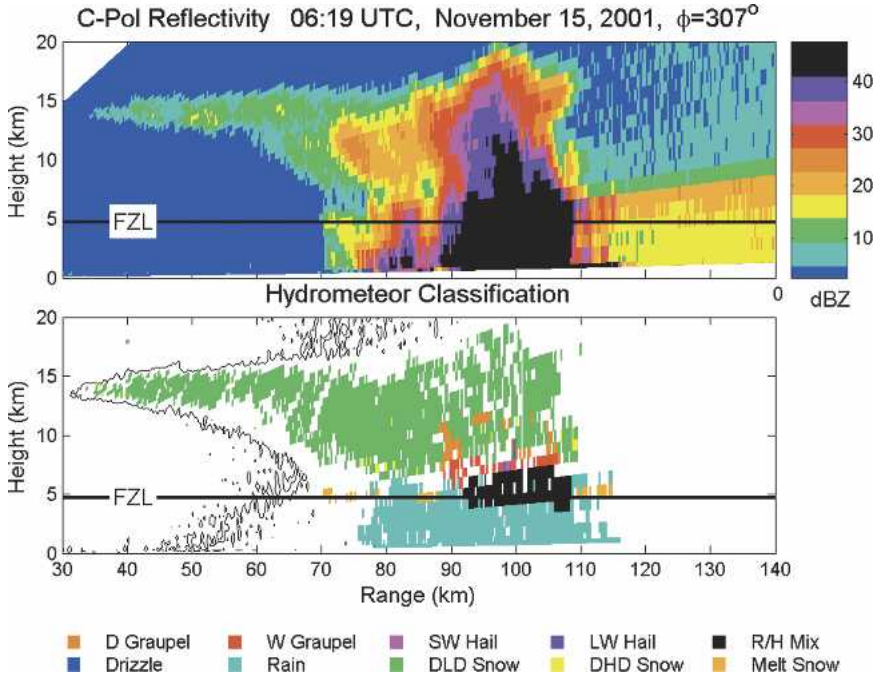

FIG. 1. RHI cross section of a thunderstorm over the Tiwi Islands north of Darwin. Note the flare echo extending behind the cell coinciding with the detection of a rain–hail mixture. The line labeled FZL is the freezing level.

cator of large, wet hail (Wilson and Reum 1988). The lower panel shows the corresponding microphysical classification, and an extensive rain–hail mixture region is seen in front of the flare. Such observations are consistent but cannot be relied on for more systematic analysis because they are fairly rare.

There has been substantial work over the past few years using wind profiler and polarimetric radar data that has demonstrated that significant hail is often present in tropical convective showers (May et al. 2001, 2002). Although hail at the surface is rare in the Tropics, the profilers at Darwin can be used to identify hail aloft. Furthermore, convection in Darwin is so frequent that a reasonable number of cases are easily collected, even though the use of profiler data means we are limited to verifying the data in a single column.

This paper will seek to verify the accuracy and limitations associated with the C-Pol retrievals in Darwin using profiler data and will examine the robustness of the fuzzy-logic retrievals themselves. The profiler comparisons will focus on hail detection, and some insights into storm dynamics and the interpretation of profiler spectra will be discussed. The latter part of this work will utilize the regular RHI scans that are performed along a cross section over the wind profiler site to look at melting snow signatures and limitations of the approach being used for the classifications in stratiform rain.

The observing network in Darwin has recently been upgraded with the addition of an ARM Program suite of instrumentation. The total observing system is probably the most complete in the Tropics. In particular, the BMRC C-Pol radar (Keenan et al. 1998) is located approximately 23 km from the two wind profilers—one operating at 50 MHz and the other at 920 MHz (Fig. 2). These systems operate routinely, and data from them are available through the ARM external data archive. Two sets of C-Pol data are available from the ARM archive. These are Cartesian grids of reflectivity and microphysical classification of the detected hydrometeors. These classifications look reasonable, but until now are essentially unverified. This paper examines some examples of these data and uses the profiler data to provide some ground truth for the microphysical classifications of the radar.

2. C-Pol radar and hydrometeor classification

The C-Pol radar runs a "volume scan" once every 10 min. These scans consist of a series of plan position indicator (PPI) sweeps at a sequence of increasing elevations. Data are sampled every 300 m out to a range of 150 km. This sampling pattern builds up a three-dimensional picture of cloud systems. Note that at 150 km the minimum detectable signal with the radar is

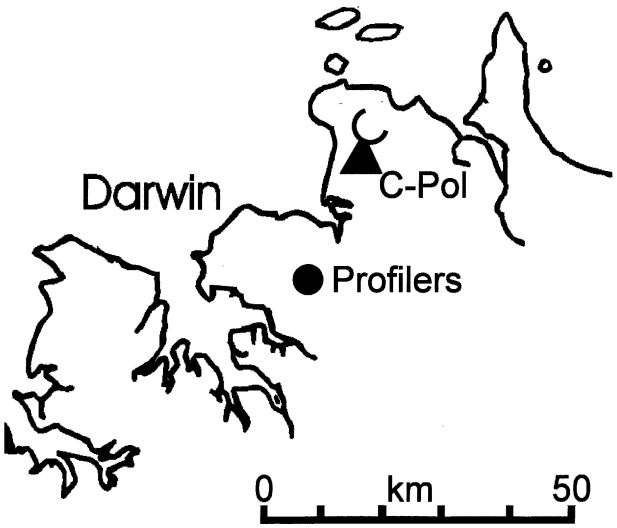

FIG. 2. Map of the Darwin area showing the locations of the C-Pol radar and the wind profilers.

about 0 dBZ, and so the radar does see substantial amounts of nonprecipitating cloud, although clearly much less than cloud radars. The volume scan data are then interpolated onto a Cartesian grid with a horizontal resolution of 2.5 km and a vertical resolution of 500 m, and a fuzzy-logic-based hydrometeor classification is performed. This horizontal resolution may seem coarse, but given that the data are collected over a 10-min volume, the spatial sampling is fairly consistent with the expected movement of a cell during the 10-min data acquisition. It is also consistent with some averaging in range for the K_{DP} estimates and averaging of the Z_{DR}s (both of these quantities are described below) to reduce their relative error and to improve the reliability of the observations (e.g., Illingworth 2003). An RHI scan is then performed at an azimuth pointing over the wind profiler site to provide high-vertical-resolution data.

The polarimetric radar alternates between horizontal and vertical polarization on a pulse-to-pulse basis. Thus, in addition to reflectivity, there are a number of additional parameters available. These parameters include the difference in reflectivity between the signals at the two polarizations [represented as the ratio Z_H/Z_V (Z_{DR})], the correlation between the signals at the two polarizations [$\rho_{HV}(0)$], and the rate of change of the differential phase on propagation (K_{DP}). The Z_{DR} is a measure of the mean oblateness of the hydrometeors. For example, large drops are oblate and produce large values of Z_{DR} (>3 dB), whereas snow and large hail tumble and have no preferred orientation so that the Z_{DR} is typically near 0 dB. The $\rho_{HV}(0)$ is near 1 for most rain but becomes substantially lower if the drops are very large (Mie scatter effects become important) or if there is mixed-phase precipitation. The K_{DP} can be understood by considering that the two polarizations essentially see different water paths because of the oblateness of raindrops and therefore one polarization is retarded relative to the other (because the refractive index is >1). In general, different hydrometeors occupy different parts of the four-dimensional phase space so that estimates of hydrometeor type can be obtained from the radar. The hydrometeor species are given in Table 1. They are not completely unambiguous, and a fuzzy-logic approach is used to combine the polarimetric estimators. An environmental temperature profile is also used, with the freezing level being the key parameter. This approach is described in detail by Straka et al. (2000) and Keenan (2003).

Following the above general principles, the classification procedure is based on the use of fuzzy-logic membership functions, with a four-step process employed to define hydrometeor species (j = 1–10). The fours steps are described in the following paragraph.

In step 1, the probability P_j^T of each hydrometeor species being present is derived based on the environmental temperature of the radar sample volume:

TABLE 1. Ranges of polarimetric variables and temperature for various hydrometeor species.

Species	Z_H (dBZ)	Z_{DR} (dB)	$\rho_{HV}(0)$	K_{DP} (° km^{-1})	Temperature (°C)
Drizzle	10–25	0.2–0.7	>0.97	0–0.06	>−10
Rain	25–60	0.5–4	>0.95	0–20	>−10
Snow (dry, low density: DLD)	−10 to 35	−0.5 to 0.5	>0.95	−1 to 1	<0
Snow* (dry, high density: DHD)	−10 to 35	0.0–1	>0.95	0–0.4	<0
Snow (wet, melting)	20–45	0.5–3	0.5–0.9	0–1	0–5
Graupel, dry (D)	20–35	−0.5 to 1	>0.95	0–1	<0
Graupel, wet (W)	30–50	−0.5 to 2	>0.95	0–3	−15 to 20
Hail, small <2 cm wet (SW)	50–60	−0.5 to 0.5	0.92–0.95	−1 to 1	−15 to 20
Hail, large >2 cm wet (LW)	55–65	−1 to 0.5	0.90–0.92	−1 to 2	−15 to 20
Rain and hail (R/H)	45–80	−1 to 6	>0.9	0–20	−10 to 25

* Rimed and aggregated snow.

$$P_j^T = P_j(T_j^{\text{lower}}, T_j^{\text{upper}}, T), \quad (1)$$

where $P_j(T_j^{\text{lower}}, T_j^{\text{upper}}, T)$ is the temperature membership function [a Gaussian bell function with 5% percentile tails is employed (Keenan 2003)], T is the temperature of the sample volume, and T_j^{lower} and T_j^{upper} represent temperature bounds from Table 1 that are considered to be consistent with the physical existence of the various hydrometeor species. In step 2, the probability P_j^R of each species is deduced based on the polarimetric variables R_k [where $k = 1, 4$ correspond to Z_H, Z_{DR}, K_{DP}, and $\rho_{\text{HV}}(0)$], using the ranges provided in Table 1:

$$P_j^R = \sum_k W_k P_j^k(R_k^{\text{lower}}, R_k^{\text{upper}}, R_k) / \sum_k W_k, \quad (2)$$

where W_k is a weighting function for each polarimetric variable (all equal to 1 in this case). In step 3, the above two probabilities are then combined to estimate P_j, the aggregated or total probability of each species:

$$P_j = P_j^T + P_j^R. \quad (3)$$

In step 4, if the maximum P_j meets the following criterion:

$$|\max(P_j) - \overline{P}| \geq 1.75\sigma_p, \quad (4)$$

where σ_P is the standard deviation of the hydrometeor class probabilities, then class j is assigned. Hence missing classification values are evident in low-confidence situations.

A Gaussian bell function structured with 5% percentile tails is employed for assigning class membership probabilities. The choice of the Gaussian bell classification function was somewhat arbitrary. It is interesting to consider how strongly these classifications are defined. Figure 3 shows histograms of the "second choice" species from the algorithms, given an estimate of rain, snow, graupel, or hail. In nearly all of the rain cases, hail is the second choice and vice versa. For snow, the second choice is generally the other snow type, which is an indication of the lack of separation in the detection phase space of the two types, or dry graupel. A similar result is seen for graupel, with the second choice being another graupel type or snow.

The fuzzy-logic process produces an estimate of weight for each of the microphysical classification types, and the strongest is selected. The ratio of the weights of the second most likely to the most likely is often very large, ~0.8 (if it were 1 there would be no difference; if it were 0 then we can be very confident in the classification). Plots of time–height cross sections of the ratio of weights and histograms of the weights (not shown) indicate that even where rain is not detected in the region below the freezing level, it is still a strong possibility. When rain is the most likely hydrometeor type, it is often, but not always, strongly selected. Likewise, snow tends to have a high probability above the freezing level even if it was not the most likely candidate. Given this observation, it is somewhat surprising that the classifications themselves are not more noisy. In fact, they seem to be internally robust despite the often high second weights (ratios >0.9). The fuzzy-logic classification procedure is undertaken either on a gate-by-gate basis in radial radar space (for RHI scans) or on a Cartesian grid (for volume scans).

An example of the radar data and the microphysical classification is shown in Fig. 1. This figure nicely shows the presence of mixed phase (mainly wet graupel and rain–hail mixtures) in the high-reflectivity areas of a thunderstorm over the Tiwi Islands, north of Darwin. This picture is consistent with the very strong updrafts in these storms lofting supercooled water and with their high level of electrical activity as hail and graupel are formed (e.g., Simpson et al. 1993).

In general the microphysical classifications of the radar seem very reasonable (Straka et al. 2000; Vivekanandan et al. 1999; Keenan 2003). However, they have not been independently verified. The remainder of this paper concerns using profilers to verify the polarimetric classification and to point out some problem areas.

3. Profiler studies of precipitation

Wind profilers have been used for the study of precipitation for more than a decade. The ability of the profilers simultaneously to observe spectral peaks associated with the clear-air vertical motion and peaks associated with hydrometeors has allowed the estimation of raindrop size distributions (e.g., Wakasugi et al. 1986), snow size distributions (Rajopadhyaya et al. 1994), and studies of the radar bright band (Drummond et al. 1996). May et al. (2001, 2002) used a combination of wind profiler and C-Pol data to examine several storms in which there was significant production of hail and graupel. In particular, the combination of 50- and 920-MHz profilers was used to sense directly the particles with fall speeds greater than the asymptotic limit for raindrops. The 50-MHz Doppler spectra are usually dominated by the clear-air echo peaks that are always seen, whereas the 920-MHz Doppler spectrum is dominated by returns from precipitation. A particularly clear example in which there is a rain–hail mixture is shown in Fig. 4. The 50-MHz spectrum shows an updraft of about 5 m s^{-1}, but the spectral peak from precipitation is not visible on a linear scale. Here, the 920-

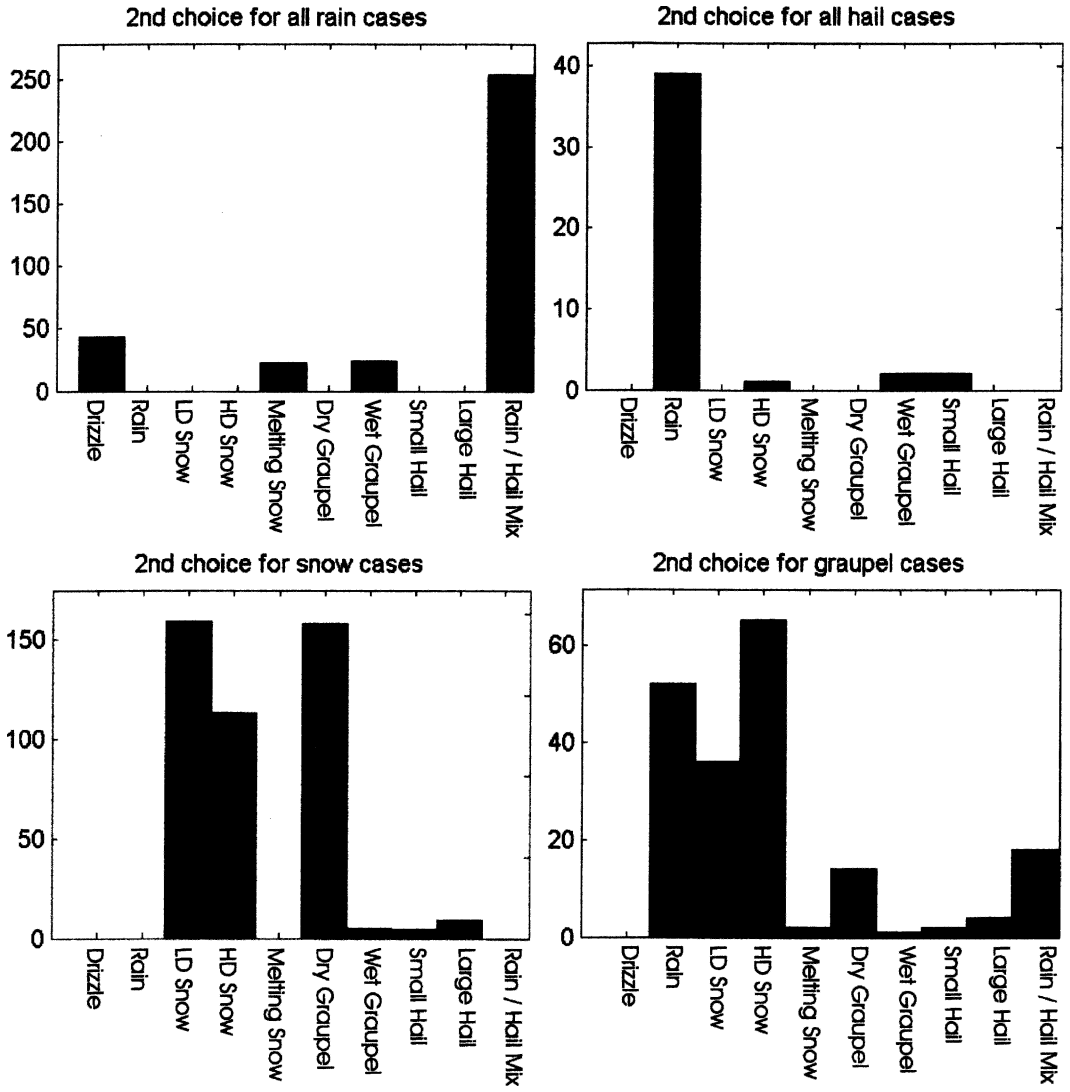

FIG. 3. Histograms of the second-choice microphysical classification for when the first choice is (top left) rain, (top right) some type of hail or rain–hail mixture, (bottom left) some type of snow, and (bottom right) some type of graupel.

MHz Doppler spectrum clearly has a distinct double-peaked structure associated with precipitation. One peak corresponds to fall speeds of about 8 m s^{-1}, which is typical of rain because the D^6 dependence of the radar cross section of individual drops weights the spectra to large raindrops with a large terminal fall speed. The second peak, at fall speeds of about 13 m s^{-1}, is only explained by the presence of 1–2-cm-sized hail. Note that the particles associated with the hail peak are ~10 times the diameter of those in the rain peak. These peaks have a similar amplitude, and so there are $\sim 10^6$ times as many drops in the rain peak as hail particles and 1000 times the water volume in the rain peak. This result illustrates the ability of the profiler to differentiate even small concentrations of wet hail. Most cases are not this clear, but both rain and hail size can be measured from the profiler data (May et al. 2002).

Remember also that the profiler vertical velocity spectra observations are taken over a period of 45 s out of a 1-min cycle, and so there may be considerable variability of the vertical motion during the data acquisition. The importance of this condition will be made clear in section 5.

One of the key tests of the C-POL classification will be the delineation of areas of mixed-phase precipitation—in particular, wet graupel and rain–hail mixtures. This condition is manifested in the profiler data as areas where there are significant signals in the profiler Dopp-

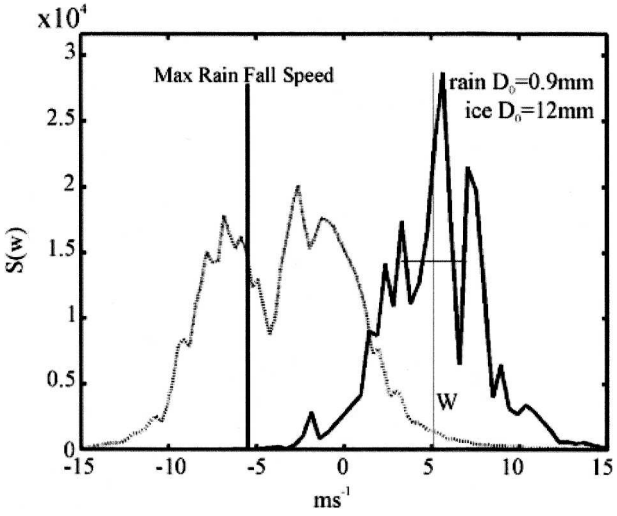

FIG. 4. Doppler spectra collected with the 50-Mhz profiler (solid) and 920-MHz profiler (dotted) at Darwin. The spectral amplitudes are arbitrarily scaled and are on a linear scale. The asymptotic limit for rain fall speeds relative to the mean air motion ($w \sim 5$ m s^{-1}) seen by the 50-MHz profiler is also included. The high fall speed peak corresponds to hail; the other is rain (after May et al. 2001).

ler spectra corresponding to particle fall speeds that are greater than the asymptotic fall speed for rain ($\sim 9.8/\rho^{0.4}$ m s^{-1}, where ρ is the air density). This spectral information allows both the detection of hail larger than about 1 cm and some size information. Note that the unambiguous detection of graupel and small hail with profiler data alone is not possible because the fall speeds are similar to that of rain.

Thus, the details of the profiler Doppler spectra and the retrievals of microphysical characteristics can clearly be used to validate the C-Pol estimates.

4. Datasets

Data from several storms passing over the profiler have been examined for hail. These storms include cases of isolated single-cell storms, continental squall lines, and monsoonal storm complexes. This choice ensures that a range of storm intensities (as defined by maximum vertical velocities) and different degrees of organization have been sampled. These cases include samples in which hail was not detected in the profiler data or only weak hail signatures were present, as well as clear hail cases. Several of the cases also had distinct trailing stratiform regions, and data collected from these regions were used to provide information for pure rain situations and to examine the difficulties of the grid-based retrievals for retrieving thin layers of melting snow. High-vertical-resolution data from RHI scans were used for this purpose.

5. Evaluation 1: A case study

Figure 5 shows an example of a time–height cross section of the profiler reflectivity, vertical motion, and reflectivity-weighted fall speed relative to the air (i.e., the vertical motion measured with the 50-MHz profiler has been subtracted from the fall speed measured with the 920-MHz profiler) through a squall line. This example shows a strong updraft on the periphery of the main precipitation core. However, this updraft is within the cloud, as demonstrated by a weak increase in the 920-MHz reflectivity (not shown). The maximum updrafts exceed 10 m s^{-1}, and it is reasonable to expect that supercooled drops are being lofted and that significant riming and potential hail production is occurring. This expectation is corroborated by the large reflectivity-weighted fall speeds seen in the downdraft in the high-precipitation area. The reflectivity-weighted fall speeds exceeded 10 m s^{-1}, which is a strong indicator that hail is present.

One intriguing feature is the apparent upward-moving precipitation next to the top of the main updraft. This feature is often seen near the top of the leading edge of convection in profiler fall speed data. Detailed examination of the radar Doppler spectra shows that there are two peaks in the 50-MHz spectrum at these altitudes. The lower-speed one is a downdraft and is the larger, but there is also a secondary upward peak to which the 920-MHz spectral peak corresponds. What appears to be happening is that there is some overturning during the 45-s data acquisition. This overturning is also indicated in the reflectivity structure with the filamentary reflectivity structure overlaying the "upward" rain. The interpretation of this observation is that the upward peak, which was probably present for only part of the 45-s record, was lofting rain and ice aloft. These particles were presumably small ones with low fall speeds so that both the 50- and 920-MHz profilers see upward motion for part of the record. However, for most of the record there was a downdraft present, as indicated by the stronger 50-MHz peak. If there was precipitation in the downdraft, it probably evaporated, perhaps intensifying the downdraft. In any case, there were no detectable echoes for the 920-MHz profiler during this part of the 45-s record. Thus, the profiler apparently sees upward-moving precipitation because the mean motion (weighted by the 50-MHz clear-air reflectivity) was downward while the precipitation echo was in the updraft portion of the record. There is also an interesting "step" in the height of the

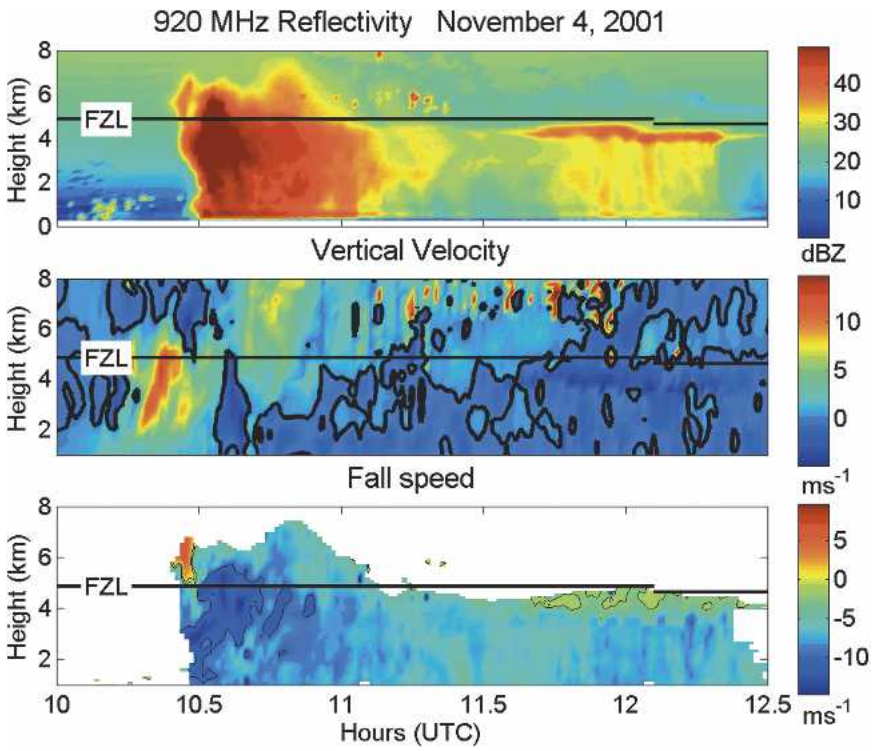

FIG. 5. Time–height cross sections of (top) the reflectivity measured with the 920-MHz profiler between 1000 and 1230 UTC 4 Nov 2001, (middle) mean vertical motion measured with the 50-MHz profiler with an overlaid contour of zero vertical motion, and (bottom) the reflectivity-weighted precipitation fall speed estimated by the difference between the Doppler velocity measured with the 920-MHz profiler and the vertical motion subtracted. The contours of the lower panel are at fall speeds of -2 and -10 m s^{-1}. The line labeled FZL is the freezing level estimated from the Darwin radiosonde ascents. Two lines are drawn because of the apparent cooling and lowering of the freezing level evident in the radar data. Soundings before and after the ascent are used.

bright band at about 1150 UTC, which is reflected in the height of the freezing level in soundings taken before and after the storm.

Figure 6 shows the corresponding time–height cross section of the C-Pol gridded reflectivity and microphysical classification data over the profiler site. This cross section has 10-min time resolution and so is, of course, much blockier than the profiler time series. The time–height cross section of the C-Pol data above the profiler is broadly consistent with the profiler data in the convective, transition, and stratiform regions of the squall line. There is a substantial region of active convection where the microphysical classification is wet graupel and rain–hail mixtures, and this region corresponds very closely to the profiler regions of large vertical velocities and high fall speed. The step from rain–hail mixtures to wet graupel, to dry graupel, and then to snow with height is consistent with the lofting of supercooled water and hydrometeor fall speed sorting, although there is some dry snow extending below the graupel that is doubtful. In general, the areas of snow and rain throughout the cross section appear to be consistent with conceptual models of such systems.

The C-Pol classifications are far from perfect, however. This fact is most in evidence in the stratiform part of the squall line (1030–1200 UTC). There is a substantial area in which there is a wet graupel classification above the melting level. This area is in the region in which the temperature is between $-10°$ and 0°C and in which aggregation of the snow crystals is likely to be occurring. Although this identification is a misclassification, it does point to the fact that microphysical data are useful in identifying significant physical processes in the precipitation. It will be shown that this result is at least partly induced by a lack of spatial resolution in the data, however.

Another problem area is the lack of a melting-snow layer in the stratiform region. The only pixels for which this occurs are in the small region where the gridded reflectivity shows a distinct brightband signature. The

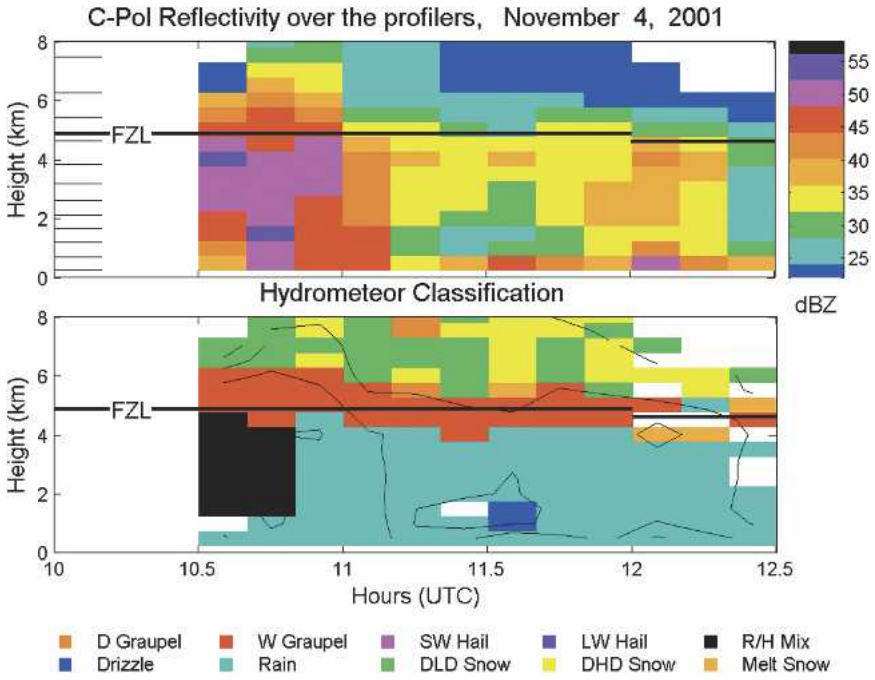

FIG. 6. Time–height cross section of (top) the C-Pol measurements of reflectivity on the grid point closest to the wind profiler location between 1000 and 1230 UTC 4 Nov 2001 and (bottom) the corresponding microphysical classification. These data are on 2.5 km × 2.5 km grids with a vertical sampling of 500 m. The actual beam heights that were used in creating these data are marked by the horizontal lines on the left of the top panel. Contours of reflectivity are overlaid on this figure. The line labeled FZL is the freezing level as in Fig. 5.

bright band is obviously much clearer in the profiler data, but the interpolation procedure used for the C-Pol data washes out this signature. This effect has been further examined by an examination of RHI data. The C-Pol radar performs an RHI scan directed over the profiler site at the end of every volume scan. The classifications for the RHI are done on a raw pixel level, and it is seen in Fig. 7 that the bright band is resolved well and that a narrow layer of melting snow comes up in the classification. Conversely, the aggregation signature of anomalous wet graupel noted in the previous paragraph is partially lost. An active convective element with a rain–hail mixture as well as a large area of wet graupel around the cell core is also evident. Thus, the melting-snow classifications where there is very good horizontal and vertical resolution appear to be fairly robust. To test whether the problem was associated with the grid resolution, the original radar volume data were resampled onto 0.5-, 1-, 1.5-, and 2-km horizontal resolution grids, and the classifications were redone. The problems that were seen in the original grids remain, however, although the sampling did produce changes in the detailed reflectivity and classification structure. Thus, the prime problem is in the limited spatial sampling in elevation inherent in volume data.

Another feature in the classification cross section is the noisiness of the region with high- and low-density snow and dry graupel above the wet graupel in Fig. 6. It is an indication that the different hydrometeor classifications are not separated well in their phase space and that the classifications of these types are uncertain. This problem is also made worse by the poor resolution and smearing inherent in the gridding of the data, because there appears to be much less noise in the snow/dry graupel classifications in the RHI data (Fig. 7). However, in this case almost no high-density snow is seen, even around the graupel areas. One recommendation arising from this result is to combine the high- and low-density snow classifications into a single snow classification.

6. Lightning echoes as validation data

Lightning may also provide an indirect confirmation of mixed-phase and graupel production in the area. Lightning echoes are seen in the profiler data. These echoes are visible as spots of very high reflectivity and spectral width and anomalous (meaningless) apparent vertical motions. They are most clearly seen in the 50-MHz data but are also visible as small bright spots in the 920-MHz reflectivity at altitudes of approximately 7–8 km just after the main peak of precipitation. These

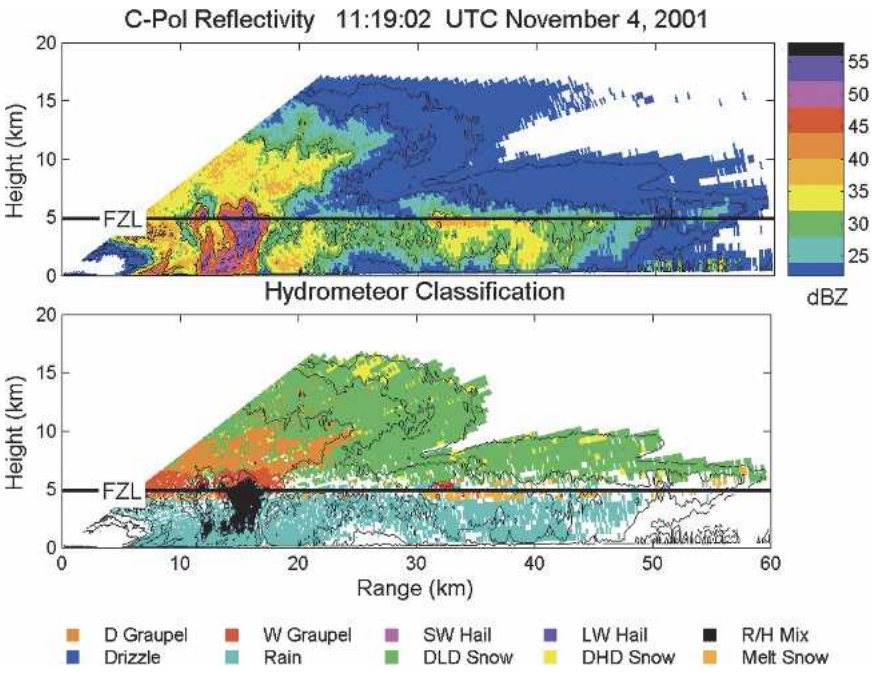

FIG. 7. RHI scan at 1119 UTC 4 Nov 2001 showing the (top) reflectivity and (bottom) classification. This figure shows an active convective element with a rain–hail mixture, as well as a large area of wet graupel around the cell core. Of particular interest here is the narrow layer of melting snow that is resolved in the stratiform region farther from the radar. Contours of radar reflectivity are overlaid on these panels. The line labeled FZL is the freezing level.

spots are not the radar seeing the direct radio emission from the lightning, because that would appear at random height, but rather are radar reflections off the ionization trail of the lightning as it is advected through the radar beam. There is also the possibility that they are being detected through sidelobes, but this possibility is argued against by their height distribution, with the most common detections just above the freezing level and near storm top, and by the fact that the echoes appear in both of the profilers at the same height (the profilers have very different sidelobes). These lightning echoes typically have very large spectral widths (covering the entire Nyquist interval so that the full width is unknown) and very high power at 50 MHz, completely masking the clear-air and precipitation spectral peaks. Such lightning echoes have been recorded in the literature (e.g., Larsen and Röttger 1987) and were discussed in detail by Atlas and Williams (2003). Atlas and Williams discussed the frequency dependence; they saw the lightning echoes with a 915-MHz profiler, but not with a 10-GHz profiler. These results illustrate that this observation can be extended to very intense echoes at 50 MHz.

Another example of the link between the profiler-detected lightning and the microphysical structure of a storm is shown in Fig. 8. It shows very nicely the occurrence of the lightning behind the initial updraft, indicating the need for some time to develop a charged mixed-phase region. It also shows the concentration of lightning detections in the layer just above the freezing level (~4.9 km) and near the storm top. The upper layer descends with the storm echo top.

These data are consistent with charging models of lightning production, with charge separation occurring where there is a mixture of graupel and ice crystals between 0° and −20°C (leading to large gradients in charge) and near the storm top, and with analyses that combine lightning detection and radar data (Williams 1989). The spatial/temporal structure is consistent with the analyses of Carey et al. (2005). Furthermore, they give credence to the classification of rain–hail mixtures and wet graupel in the region of the lightning occurrence. These signatures are much weaker in oceanic convection (to be discussed next) when there is little lightning activity (Williams et al. 1992).

7. Systematic evaluation of the classifications

The previous sections have discussed some case studies illustrating the qualitative consistency between the profiler observations and the polarimetric classifications. To put it onto a more quantitative basis, the pro-

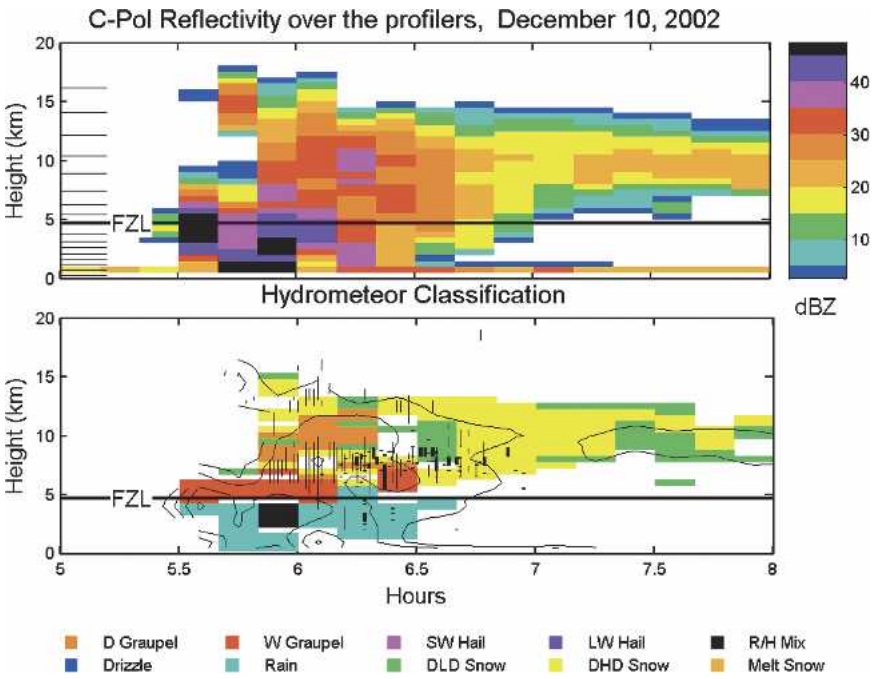

FIG. 8. Another time–height cross section of the reflectivity and classifications for 0500–1000 UTC 10 Dec 2002. In this case, however, the locations of lightning echoes in the profiler data have been overlaid (vertical lines) along with contours of reflectivity as before. The heavier lines mark the times and heights for which lightning echoes are evident in the 920-MHz data as well as in the 50-MHz data. This case was very electrically active, although the most intense convection missed the profiler. An extensive region of wet graupel is visible prior to and in the electrically active period, however. The line labeled FZL is the freezing level.

filer data were sorted into time–height cross sections of the reflectivity from the rain and hail components separately and then were mapped onto the polarimetric sampling. That is, a profiler hail detection was flagged if significant "hail" was seen at a given height range during the first 6 min of the 10-min volume scan. This approach was to allow for the scanning time and the spatial averaging inherent in the volume estimate. This procedure was performed and columns of detections were compared for six cases that totaled more than 10 h of precipitation over the profiler. Two of these cases were from monsoonal convection where the vertical motions were expected to be much weaker, although one (17 February 2003) had a clear hail signature in both datasets. This choice was to provide a test for the nonoccurrence of the hail signatures in convection with high rainfall rates but weak vertical motions and little hail expected to develop. In these monsoon cases, little or no hail signatures were seen in either dataset.

An event was classed as a detection if there was a hail signature present in the column for a given 10-min interval within the six time series. The results are summarized in Table 2. There were eight hits, two misses, and two false alarms in over 10 h of data for which precipitation was over the profiler. Of the two misses, one sample only had hail in the small part of the 10-min cycle, and this part was adjacent to a clear hit. The second miss had only a weak signature in the profiler data with relatively low reflectivity. This sample may be a false detection by the profiler. Of the false alarms, one was only a single pixel in a relatively low reflectivity time–height cross section and so is likely a classification error, and the other was adjacent to a very strong detection. Although tagged as a false alarm, it is very likely that there was hail present in the 2.5 km $\times$ 2.5 km volume and the false alarm is a product of the spatial sampling of the C-Pol data.

8. Conclusions

Some cases of convective storms have been examined using the combination of the wind profiler and polarimetric radar data. Of these cases, several highlight the large overturning and entrainment at the top of the leading edge of convection in the profiler data, including the case examined in detail in this paper. The profiler data are clearly useful in verifying the C-Pol microphysical classifications. Furthermore, the classifica-

TABLE 2. Summary of hail detections over 6 cases.

Date	Time of C-Pol detection (UTC)	Comment	Time of profiler detection (UTC)	Comment
4 Nov 2001	1030		1030	
	1040			False alarm because of spatial averaging?
17 Nov 2001			0930	Leading edge midway through 10 min.
	0940		0940	
10 Feb 2002	0550		0550	
			0600	Low Z, scattered in height.
5 Feb 2003	0450		0450	
	0500	Weak, scattered in height.	0500	Weak, scattered in height.
16 Feb 2003	1250	Single pixel.		
17 Feb 2003	1750		1750	
	1800		1800	
	1810		1810	

tions of rain–hail mixtures themselves are remarkably robust. The number of false alarms and missed detections was very low considering the limited data available, the fact that gridded data were used, and the limited separation in the measurement phase space of different hydrometeor combinations.

One area of concern in the basic method is the attempt to define too many closely separated classifications. This problem is seen clearly in Figs. 6 and 7. These figures indicate that the high- and low-density snow classifications should be combined into a single snow classification.

Performing classifications on the gridded data is not ideal. This fact is particularly evident in stratiform rain with a bright band where the radar signatures are smeared in the gridding process. It results in two problems. One is an apparent layer of wet graupel above the melting level that is probably erroneous. It may be related to aggregation of the ice crystals but is more likely a weakness in the classification because a similar signature does not appear in the RHI data. The other problem is the lack of detection of melting snow. These problems may be alleviated by applying the classification to the raw data and then gridding the classifications or by using the full three- or four-dimensional information available to refine and edit the classification fields. The former faces some problems on how to perform the interpolation of the classifications onto a grid.

The C-Pol dataset will be very useful in placing the ARM cloud data in context with respect to the cloud origin and the characteristics of the parent convection. These gridded data are being made available as an external dataset to the ARM community, as are the profiler data (available online at the time of writing at http://www.arm.gov).

Acknowledgments. This work is partly supported by the U.S. Department of Energy Atmospheric Radiation Measurement Program. The Darwin 920-MHz profiler belongs to the Aeronomy Laboratory of NOAA.

REFERENCES

Atlas, D., and C. R. Williams, 2003: Radar echoes from lightning and their microphysical environment. *Geophys. Res. Lett.,* **30,** 1262, doi:10.1029/2002GL016521.

Carey, L. D., M. J. Murphy, T. L. McCormick, and N. W. S. Demetriades, 2005: Lightning location relative to storm structure in a leading-line, trailing-stratiform mesoscale convective system. *J. Geophys. Res.,* **110,** D03105, doi:10.1029/2003JD004371.

Drummond, F. J., R. R. Rogers, S. A. Cohn, W. L. Ecklund, D. A. Carter, and J. S. Wilson, 1996: A new look at the melting layer. *J. Atmos. Sci.,* **53,** 759–769.

Illingworth, A., 2003: Improved precipitation rates and data quality by using polarimetric measurements. *Weather Radar*, P. Meischner, Ed., Springer Verlag, 130–166.

Keenan, T. D., 2003: Hydrometeor classification with a C-band polarimetric radar. *Aust. Meteor. Mag.,* **52,** 23–31.

——, K. Glasson, F. Cummings, T. S. Bird, J. Keeler, and J. Lutz, 1998: The BMRC/NCAR C-band polarimetric (C-POL) radar system. *J. Atmos. Oceanic Technol.,* **15,** 871–886.

Larsen, M. F., and J. Röttger, 1987: Observations of thunderstorm reflectivities and Doppler velocities measured at VHF and UHF. *J. Atmos. Oceanic Technol.,* **4,** 151–159.

May, P. T., A. R. Jameson, T. D. Keenan, and P. E. Johnston, 2001: A comparison between polarimetric radar and wind profiler observations of precipitation in tropical showers. *J. Appl. Meteor.,* **40,** 1702–1717.

——, ——, ——, ——, and C. Lucas, 2002: Combined wind profiler/polarimetric radar studies of the vertical motion and microphysical characteristics of tropical sea breeze thunderstorms. *Mon. Wea. Rev.,* **130,** 2228–2239.

Rajopadhyaya, D. K., P. T. May, and R. A. Vincent, 1994: Retrievals of ice particle size distributions from VHF wind profiler Doppler spectra. *J. Atmos. Oceanic Technol.,* **11,** 1559–1568.

Schuur, T., A. Ryzhkov, P. Heinselman, D. Zrnic, D. Burgess, and K. Scharfenberg, 2003: Observations and classification of echoes with the polarimetric WSR-88D radar. NSSL Rep., 46 pp.

Simpson, J., T. D. Keenan, B. Ferrier, R. H. Simpson, and G. J. Holland, 1993: Cumulus mergers in the maritime continent region. *Meteor. Atmos. Phys.,* **51,** 73–99.

Straka, J. M., 1996: Hydrometeor fields in a supercell storm as deduced from dual-polarization radar. Preprints, *18th Severe Local Storms Conf.,* San Francisco, CA, Amer. Meteor. Soc., 551–554.

——, D. Zrnic, and A. Ryzhkov, 2000: Bulk hydrometeor classification and quantification using polarimetric radar data: Synthesis of relations. *J. Appl. Meteor.,* **39,** 1341–1372.

Vivekanandan, J., D. S. Zrnic, S. M. Ellis, R. Oye, A. V. Ryzhkov, and J. Straka, 1999: Cloud microphysics retrieval using S-band dual-polarization radar measurements. *Bull. Amer. Meteor. Soc.,* **80,** 381–388.

Wakasugi, K., A. Mizutani, M. Matsuo, S. Fukao, and S. Kato, 1986: A direct method for deriving drop-size distribution and vertical air velocities from VHF Doppler radar spectra. *J. Atmos. Oceanic Technol.,* **3,** 623–629.

Williams, E. R., 1989: The tripole structure of thunderstorms. *J. Geophys. Res.,* **94,** 13 151–13 167.

——, S. A. Rutledge, S. G. Geotis, N. Renno, E. Rasmussen, and T. Rickenbach, 1992: A radar and electrical study of tropical "hot towers." *J. Atmos. Sci.,* **49,** 1386–1396.

Wilson, J. W., and D. Reum, 1988: The flare echo: Reflectivity and velocity signature. *J. Atmos. Oceanic Technol.,* **5,** 197–205.